AIAA JOURNAL
Vol. 39, No. 5, May 2001

Solution Adaptation of Unstructured Grids for Two-Dimensional Aerodynamic Computations

P. C. Walsh* and D. W. Zingg†
University of Toronto, Downsview, Ontario M3H 5T6, Canada

A solution-adaptive gridding technique applicable to the numerical solution of the Navier–Stokes equations using unstructured triangular grids is presented and evaluated. Grid adaptation is directed by a parameter based on undivided differences of density and Mach number normalized with their respective grid extrema. A new solution-dependent retriangulation algorithm locally restructures the grid to recover an anisotropic grid following adaptation. The artificial dissipation operator is modified to provide improved accuracy on irregular high aspect ratio triangular grids that may be created in some regions by the adaptive process. The technique is applied to several subsonic and transonic turbulent aerodynamic flows, including the flow over a three-element, high-lift configuration. Grid convergence studies are presented that demonstrate that the grid adaptation procedure leads to significant error reduction in lift and drag coefficient in most circumstances. The effectiveness of the adaptation is significantly improved as a result of the solution-dependent retriangulation and the improved artificial dissipation operator.

Nomenclature

A_i	=	area of control volume i
E	=	total energy per unit mass
e	=	grid edge index
F, G	=	total flux in x and y directions
l	=	grid edge length
M	=	Mach number
N	=	total number of nodes in grid
S	=	stretching parameter
t	=	time
u, v	=	Cartesian velocity components
$\delta\Omega$	=	arbitrary control volume boundary
$\tilde{\nu}$	=	turbulence variable
ρ	=	density
Φ	=	adaptation parameter
ω	=	solution vector, $[\rho\ \rho u\ \rho v\ \rho E\ \rho\tilde{\nu}]^T$
Ω	=	arbitrary control volume

Introduction

TO increase the usefulness of computational methods in aerodynamic design, the time required for problem setup and solution must be reduced. Solution-adaptive grid strategies can play a significant role in achieving this goal. First, adaptive gridding can lead to a reduction in the number of grid nodes required to achieve specified accuracy levels, thus saving computing time and memory. Second, adaptive gridding can decrease the user expertise and effort required to produce a satisfactory simulation by reducing the dependence on the grid used to initiate the process. Although the first area has received the most emphasis to date,[1] the second area, reduction of expertise and effort in grid generation, may prove to be the more important benefit of solution-adaptive gridding in the long run.[2] Unstructured grids have great potential for achieving the two goals of adaptation described, especially when complex geometries are involved, as a result of their superior flexibility with respect to node addition. Whereas unstructured grid adaptation can be very successful for inviscid flows,[3–5] turbulent aerodynamic flows at high Reynolds number are more challenging, primarily because the highly anisotropic nature of such flows requires a correspondingly anisotropic grid.[6,7] Grid cells with high aspect ratios increase the difficulty of point insertion and connection and can adversely affect the accuracy of the spatial discretization.[8] This has motivated the use of hybrid grids combining a semistructured grid in boundary layers and wakes with a fully unstructured grid elsewhere. Whereas this approach can be advantageous, it is also restrictive in terms of the adaptation of the semistructured portion of the grid. In such regions, grid quality can deteriorate through repeated refinements unless restrictions are placed on the configuration of the resulting cells.[9]

As a result of the difficulties associated with turbulent aerodynamic flows, there exist few studies demonstrating the benefits of solution-adaptive gridding for such flows in a quantitative manner. Quantitative studies are essential to determine the cost effectiveness of an adaptive-gridding technique and to perform parameter optimization. One such investigation is presented in Ref. 10 for an adaptive grid redistribution scheme applied to Navier–Stokes computations of steady airfoil flows using structured grids. Using baseline solutions computed on very fine grids, this study shows that the error reduction resulting from adaptive grid redistribution is quite modest due to the conflicting requirements of grid clustering and smoothness.

The purpose of the present paper is to present and quantitatively assess a solution-adaptive gridding technique based on triangular unstructured grids in the context of two-dimensional aerodynamic flows. Progress has been made in both the quality of the adapted grid and the accuracy of the discretization on the adapted grids. In the former area, a solution-dependent retriangulation scheme is used to restructure the adapted grid consistent with the local flow conditions. In the latter area, the artificial dissipation operator has been modified to produce improved accuracy for highly stretched cells. Grid convergence studies are presented to quantify the effectiveness of the approach. Our interest here is in numerical error, specifically discretization error, as opposed to physical-model error, for example, the turbulence model. Hence, the errors are determined by comparison with accurate numerical solutions rather than experimental data. Furthermore, the error reduction associated with the grid adaptation technique is evaluated not by comparison with solutions computed on globally fine grids (which are obviously inferior in terms of cost effectiveness) but by comparison with solutions computed on grids with appropriate clustering as would be generated by an experienced user without specific knowledge of the solution. Finally, the solution-adaptive gridding technique is studied and evaluated using an explicit multigrid solver, but can be used equally effectively with other approaches, such as implicit solvers.

Received 31 August 1998; revision received 15 September 2000; accepted for publication 17 October 2000.

*Graduate Student, Institute for Aerospace Studies; currently Assistant Professor, Department of Mechanical Engineering, Ryerson Polytechnic University, 350 Victoria Street, Toronto, ON M5B 2K3, Canada.

†Professor, Institute for Aerospace Studies, 4925 Dufferin Street. Member AIAA.

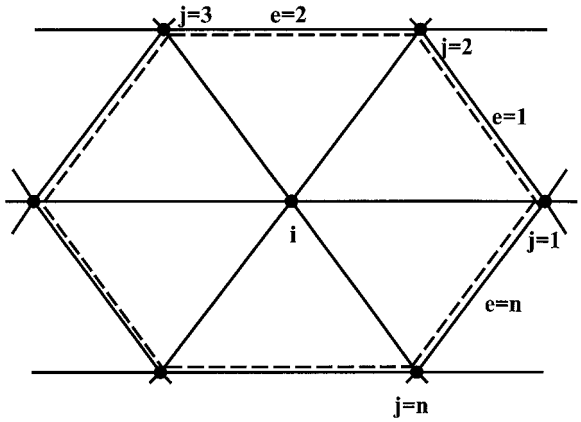

Fig. 1 Typical control volume.

Numerical Algorithm

The Navier–Stokes equations, describing the behavior of compressible viscous flows, are given in integral form for a control volume Ω bounded by the closed contour $\delta\Omega$ as

$$\frac{\mathrm{d}}{\mathrm{d}t}\int_{\Omega}\omega\,\mathrm{d}x\,\mathrm{d}y+\oint_{\partial\Omega}(F\,\mathrm{d}y-G\,\mathrm{d}x)=0 \tag{1}$$

where the variables are defined in the Nomenclature. The numerical solution of the conservation equations is performed over control volumes composed of an arbitrary number of triangular cells, as shown in Fig. 1. Each control volume consists of a central node i and an arbitrary number of neighbor nodes, the location of which defines the boundary of the control volume, shown as a dashed line. Data values are associated with the nodes of the grid, yielding a node-centered scheme with overlapping control volumes, as developed and popularized by Jameson et al.[11] Dependent variables are considered to be cell averages, reducing Eq. (1) to a discrete form:

$$\frac{\mathrm{d}\omega_i}{\mathrm{d}t}=-\frac{1}{A_i}\sum_{e=1}^{n}(F\Delta y-G\Delta x)_e \tag{2}$$

The fluxes F and G are evaluated using linear interpolation along each edge e. The discretized equations are time marched to a steady state through a five-stage Runge–Kutta scheme. Convergence acceleration is achieved through local time stepping, residual smoothing, and the multigrid technique. The effects of turbulence are introduced through the one-equation Spalart–Allmaras eddy viscosity model.[12]

Numerical dissipation is required to control nonlinear instability and to damp unresolved high-frequency modes. The required dissipation is added through a combination of undivided Laplacian and biharmonic approximations[13] applied to dependent variables. The Laplacian approximation is used in regions of discontinuous flow, such as near shock waves, where a greater degree of dissipation is required. In areas of smooth flow, the biharmonic operator is used.

The adaptive-gridding routine creates increased irregularity in the unstructured grids as new nodes are introduced in selected regions. The artificial dissipation scheme should be constructed in such a manner as to maintain a higher-order approximation to the undivided Laplacian operator, regardless of the degree of irregularity or of local grid stretching. Such an operator is constructed by the following discretization of the undivided Laplacian of the dependent flow variables[14]:

$$\mathrm{d}(\omega)_i=\phi_i\sum_{e=1}^{n}(\omega_x\Delta y-\omega_y\Delta x)_e \tag{3}$$

The values Δx and Δy are obtained from the edges forming the control volume boundary. The first derivatives, ω_x and ω_y, are determined on the triangular cells internal to the given control volume associated with the edge. As desired, this operator produces no dissipation for a locally linear solution, even on an irregular grid. However, for nonlinear solutions on highly stretched grids, excessive dissipation can be produced. The following scaling factor ϕ_i is added to correct this:

$$\phi_i=\left[\sum_{j=1}^{n}\frac{2\,\mathrm{area}_{j,j+1}}{l_{j,j+1}^2}\right] \tag{4}$$

The term $l_{j,j+1}$ is the length of an outer edge joining nodes j and $j+1$ with $\mathrm{area}_{j,j+1}$, the area of the triangular cell internal to the given control volume associated with the edge. The biharmonic operator is constructed using simple edge differences:

$$\mathrm{d}^2(\omega_i)=\sum_{j=1}^{n}[\mathrm{d}(\omega)_j-\mathrm{d}(\omega)_i]_j \tag{5}$$

where indices j and i are consistent with Fig. 1. The details of this method have been presented by Walsh and Zingg.[15,16]

Adaptive-Gridding Technique

The approach taken here follows the following sequence:

1) Begin with a very coarse grid and obtain a moderately converged flow solution.

2) Based on an adaptation parameter, identify regions requiring increased resolution.

3) Place the values of the adaptation parameter and the corresponding edges in descending order and subdivide sequentially using a two-pass procedure.

4) Retriangulate and smooth the new grid.

5) Obtain a moderately converged solution on this grid and repeat, or continue to convergence and terminate.

Steps 2, 3, and 4 are described in more detail.

The adaptation parameter used is based on undivided differences of density and Mach number normalized with the largest such difference on the grid:

$$\Phi=\frac{|\rho_1-\rho_2|}{\rho_{\max}-\rho_{\min}}+\frac{|M_1-M_2|}{M_{\max}-M_{\min}} \tag{6}$$

Here, locations 1 and 2 are the nodes at each end of a given edge. Any flowfield variable or combination of variables can serve as an adaptation parameter. For inviscid flows, Dannenhoffer and Baron[3] found that adaptation based on undivided differences of density required the smallest computational expense for a given level of accuracy. In laminar and high Reynolds number flows, Walsh and Zingg[16] and Walsh[17] have shown quantitatively that an adaptation parameter based on undivided differences of density and Mach number is effective for a variety of flow types.

For the adapted grid to be used with the original grid in the multigrid sequence, we desire a roughly fourfold increase in the number of nodes.[18,19] If this were done in one pass, all edges would be subdivided, leading to an inefficient global refinement. Instead, we subdivide the edges in two passes, with 55% of the nodes added in the first pass and 45% of the nodes added in the second pass. Hence, a triangle on the initial grid can be subdivided into 16 smaller triangles in one application of the adaptation procedure. Detailed studies presented in Ref. 17 demonstrate that this is an efficient approach. A limitation of this approach is that it preserves the cell aspect ratios of the initial grid. Although this avoids the difficulties associated with the possibility of excessively high cell aspect ratios, it does require that the initial grid must be reasonably appropriate in terms of cell aspect ratio. Boundary edges are selected and adapted based on the curvature criterion developed by Mavriplis.[20]

Once a new adapted grid is generated, the edge orientation usually results in irregularly shaped control volumes, potentially leading to large increases in the spatial discretization error. In grid generation algorithms, the minmax criterion is used to impart regularity to meshes. The minmax criterion is satisfied locally when an edge shared between two triangles is oriented such that the largest interior angle of the two triangles is minimized.[21] Edges are swapped over the entire grid in an iterative process until this criterion is met. In inviscid regions, the minmax edge swapping routine is very successful at recovering a smooth grid. However, in regions with high aspect ratio cells, use of the minmax retriangulation following adaptive node placement can lead to undesirable grid characteristics. Adaptive gridding will add nodes in these anisotropic regions, and subsequent minmax retriangulation will destroy the locally anisotropic

nature of the grid. To prevent such undesirable retriangulations, the grid can be locally stretched in the direction of the prevailing Mach number gradient before the minmax algorithm is implemented. The resulting retriangulation will not destroy the high aspect ratio nature of the local grid. In fact, this method is solution dependent, conforming to the character of the local flowfield.

Initially, the gradient of the Mach number is computed and averaged over the four nodes of a pair of triangles that share a common edge (M_x M_y). A stretching parameter S is then formed and used to place temporarily the four nodes into their stretched locations before the minmax criterion is locally enforced. It is given by

$$S = \left[\frac{(M_x \Delta x + M_y \Delta y) + \varepsilon}{|M_x \Delta x + M_y \Delta y + \varepsilon|} l^2 C \right] \tag{7}$$

$$X_i^1 = X_i^o + (M_x / M_\infty) S \tag{8}$$

$$Y_i^1 = Y_i^o + (M_y / M_\infty) S \tag{9}$$

The lengths Δx and Δy are the distances from the midpoint of the edge to the neighbor nodes of the quadrilateral under consideration. Here the superscript 1 refers to the location in the stretched space and o refers to the original location. The parameter l is the edge length, and C is a stretching coefficient, set to a value of 2.0. The term ε is set to 10^{-6} to prevent singularities, and M_∞ is the freestream Mach number. The stretched retriangulation scheme is imposed following adaptive node insertion in an iterative fashion until the entire grid conforms to a minmax criterion in stretched space. Following adaptation and retriangulation, the isotropy desired in the inviscid regions may be disrupted. An isotropic grid in smooth flow can reduce local truncation error,[17,21] prompting the use of a postprocess smoother. Several iterations of explicit Laplacian smoothing are applied after retriangulation. Although this smoothing procedure addresses the isotropy in the inviscid regions, it has the potential to reduce the anisotropy imposed in the retriangulation process. Therefore, the smoothing perturbation is attenuated by the reciprocal of the aspect ratio, effectively confining its influence to the inviscid regions.

The influence of stretched retriangulation is clearly demonstrated in Figs. 2–4. An unadapted grid with a total of 800 nodes is shown in Fig. 2, and an adapted grid with the standard minmax retriangulation is shown in Fig. 3. The triangulation procedure sporadically creates nearly equilateral cells in the boundary-layer regions. With the modified minmax retriangulation shown in Fig. 4, the adapted grid retains the locally anisotropic nature desired in the boundary layer.

Results and Discussion

Four test cases are used to assess the adaptive gridding technique, the modified dissipation operator, and the retriangulation scheme. These include 1) a laminar flow over the NACA 0012 airfoil, 2) a subsonic turbulent flow over the NACA 0012 airfoil, 3) a transonic turbulent flow over the RAE 2822 airfoil, and 4) a subsonic turbulent flow over a three-element, high-lift geometry typical of a takeoff configuration. Details are given in Table 1 (see Refs. 10 and 22–25). For the first two cases, the adapted grids are assessed quantitatively using very fine grids as benchmark solutions for error estimation. For cases 3 and 4, results obtained using a well-established flow solver on structured grids with a high node density are used for comparison.

For the first case, we begin by considering the solution on a sequence of five successively refined unadapted grids with the characteristics given in Table 2. The lift and drag coefficients computed

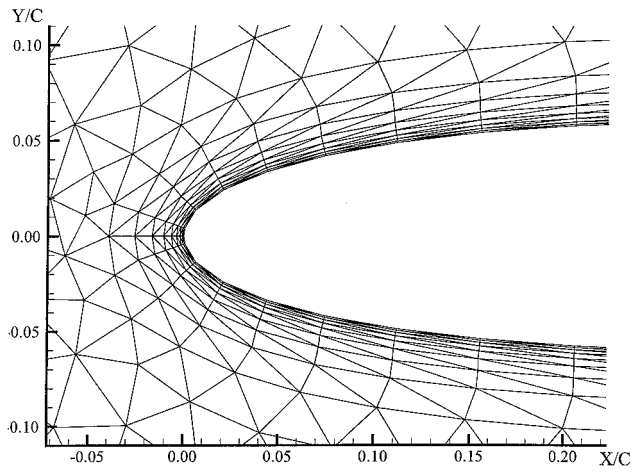

Fig. 2 Unadapted grid; 800 nodes.

Table 1 Test case summary

Test case	Airfoil	Mach number	Angle of attack, deg	Reynolds number	Reference
1	NACA 0012	0.8	10.0	500	22
2	NACA 0012	0.16	6.0	2.88×10^6	10
3	RAE 2822	0.729	2.70	6.5×10^6	23
4	AGARD AR 303 A2	0.197	4.0	3.52×10^6	24, 25

Table 2 Grids for case 1

Grid	Total nodes	Nodes on body	Off-wall spacing
1	752	60	0.01
2	2,736	120	0.005
3	10,769	240	0.0025
4	39,635	480	0.00125
5	78,459	960	0.000625

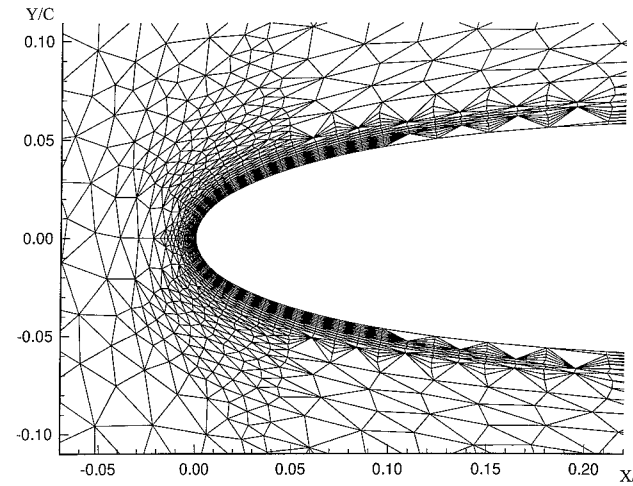

Fig. 3 Adapted grid, standard minmax retriangulation; 2800 nodes.

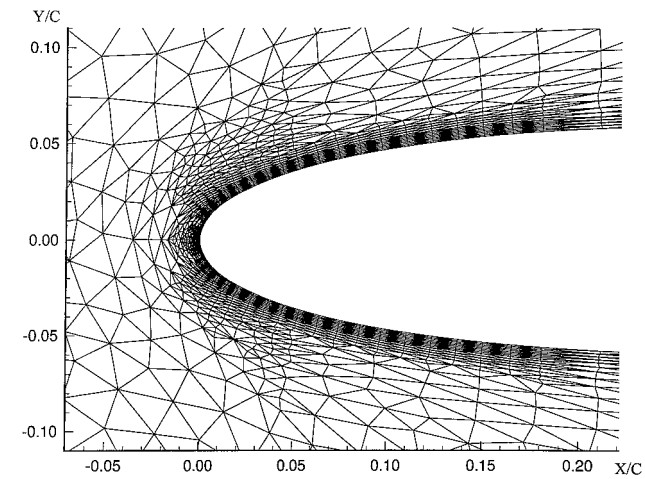

Fig. 4 Adapted grid, modified minmax retriangulation; 2800 nodes.

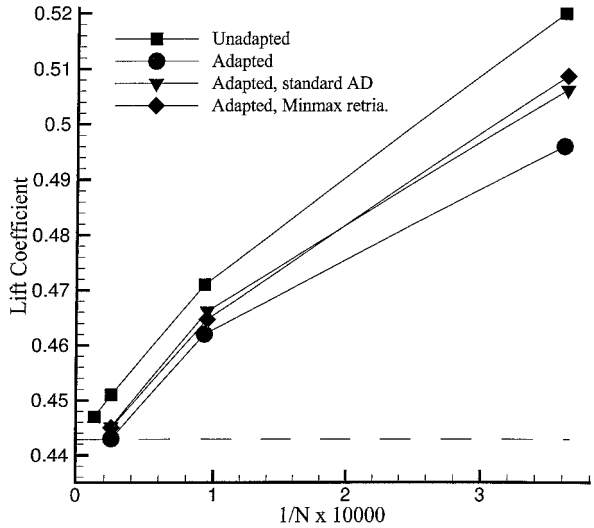

Fig. 5 Lift coefficients produced by adapted and unadapted grids for case 1; dashed line is grid-independent solution obtained through Richardson extrapolation.

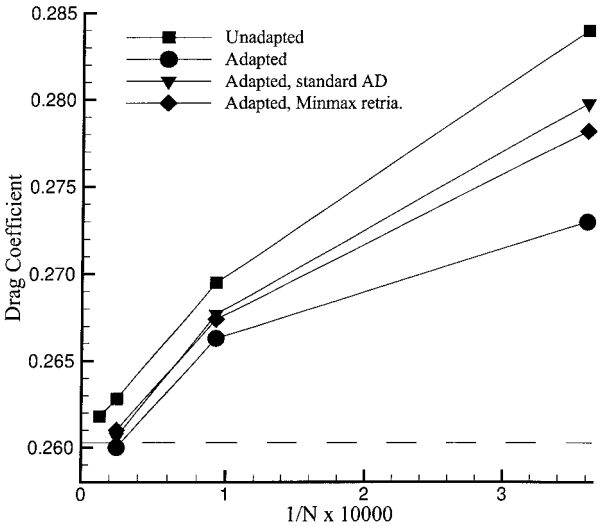

Fig. 6 Drag coefficients produced by adapted and unadapted grids for case 1; dashed line is grid-independent solution obtained through Richardson extrapolation.

on the four finest of these grids are plotted in Figs. 5 and 6, respectively, as a function of the reciprocal of the number of nodes in the grid. The linear variation seen for the finest three unadapted grids is indicative of the second-order behavior of the solver under global refinement. Thus, one can estimate grid-independent values of the lift and drag coefficients with some confidence using Richardson extrapolation.

Next we apply the adaptation procedure to grids 1, 2, and 3, producing a fourfold increase in the number of nodes in each case, leading to adapted grids with overall grid densities comparable to grids 2, 3, and 4, respectively. Results for these adapted grids are also shown in Figs. 5 and 6, where N corresponds to the number of nodes in the grids after adaptation. The grid-independent solution obtained through Richardson extrapolation is represented by the dashed line in both of Figs. 5 and 6. In each case, the error produced by the adapted grid is substantially reduced in comparison with the unadapted grid with a comparable number of nodes. In fact, the adapted grid with roughly 40,000 nodes produces lift and drag coefficients that are closer to the extrapolated grid-independent values than those computed on the unadapted grid with twice as many nodes. The computational cost for producing an adapted grid for this case was approximately 5% of the total cost of a converged solution.

Figures 5 and 6 also provide an assessment of the solution-dependent retriangulation scheme and the artificial dissipation operator. Two additional sets of adaptive results were also obtained.

Table 3 Grids for case 2

Grid	Total nodes	Nodes on body	Off-wall spacing
1	3,415	180	0.001
2	5,768	240	0.00005
3	13,751	360	0.000032
4	22,062	480	0.000015
5	84,521	960	0.000005

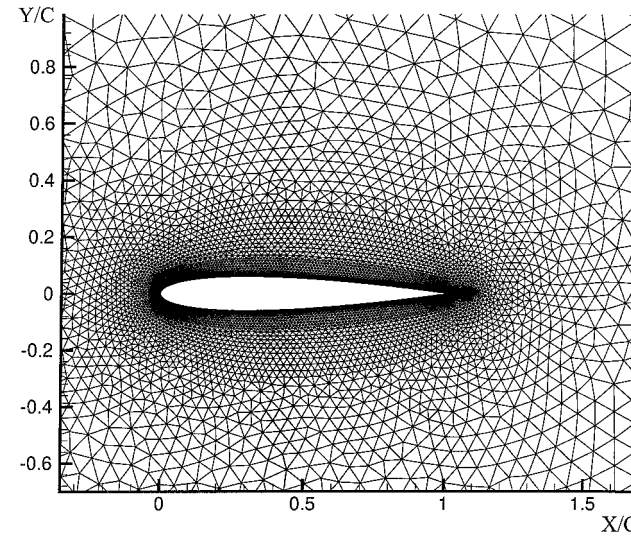

Fig. 7 Unadapted grid with roughly 10,000 nodes; case 1.

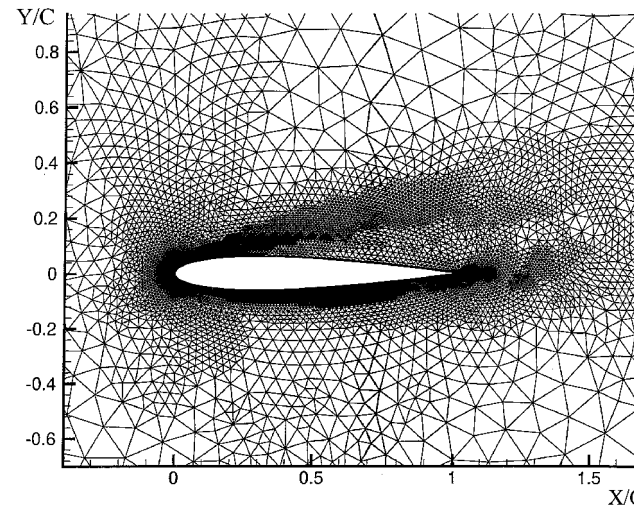

Fig. 8 Adapted grid with roughly 10,000 nodes; case 1.

One uses an artificial dissipation operator based on simple edge differences akin to Eq. (5) denoted as standard AD, along with the solution-dependent retriangulation scheme. The other, denoted as minmax retria., uses the higher-order dissipation scheme but with minmax retriangulation only, without prestretching. The results of these two cases lie between those of the unadapted and adapted results, which shows that both higher-order dissipation and solution-dependent retriangulation improve the effectiveness of the adaptation scheme.

Figures 7 and 8 compare the unadapted and adapted grids with roughly 10,000 nodes, which are quite dissimilar. It is clear that the unadapted grid is far from optimal for this case, and furthermore, it is equally clear that it would be virtually impossible to generate a grid such as the adapted grid without knowledge of the solution.

A similar quantitative assessment is performed for test case 2, which requires a much more anisotropic grid than case 1 because the Reynolds number is much higher and the flow is turbulent. Again, a sequence of five unadapted grids is generated with the characteristics

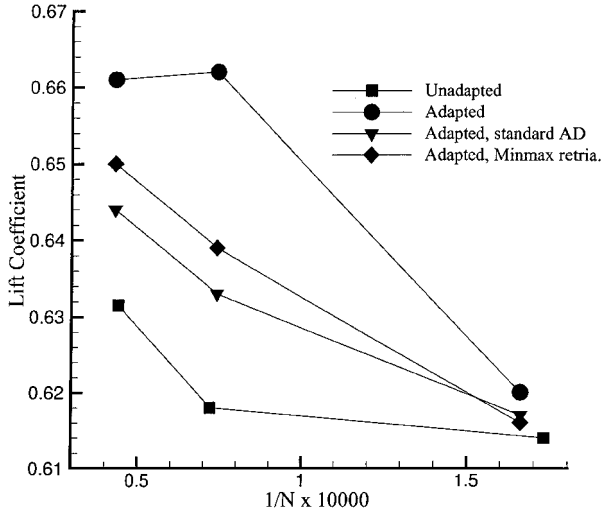

Fig. 9 Lift coefficient produced by adapted and unadapted grids; case 2.

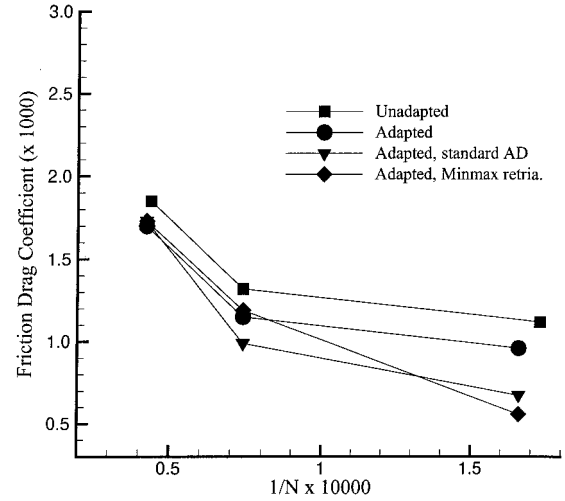

Fig. 11 Friction drag coefficient produced by adapted and unadapted grids; case 2.

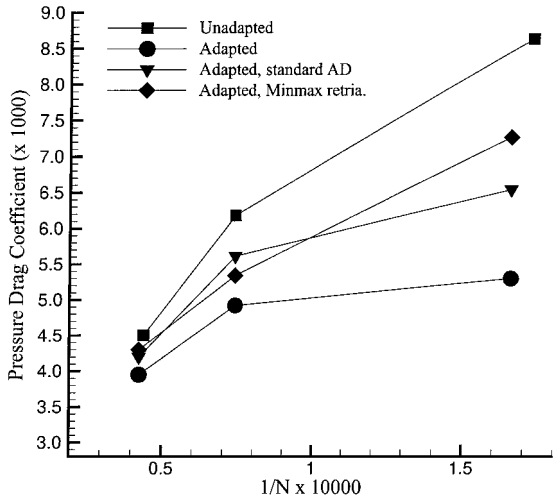

Fig. 10 Pressure drag coefficient produced by adapted and unadapted grids; case 2.

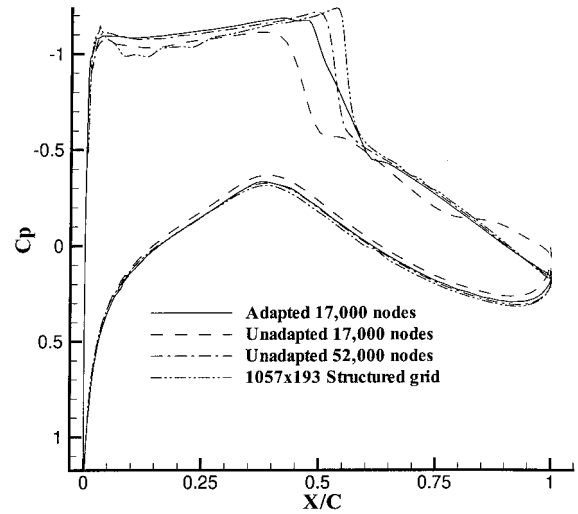

Fig. 12 Surface pressure coefficient; case 3.

shown in Table 3. Adapted grids are produced from grids 1, 2, and 3 in the sequence, with grid densities similar to grids 2, 3, and 4, respectively. The computed lift coefficients are shown in Fig. 9, and the pressure and friction drag coefficients are shown in Figs. 10 and 11, respectively. Similar to case 1, the adaptation achieves the greatest error reduction when higher-order artificial dissipation and solution-dependent retriangulation are used. The reduction in error in both lift and pressure drag is significant. However, no improvement in friction drag is seen in Fig. 11, as a result of difficulties with the spatial discretization on nonsmooth high-aspect-ratio triangular grids. Further work is needed to address the error in friction drag.

For the third test case, consisting of a transonic turbulent flow over the RAE 2822 airfoil, we rely on numerical results computed using a higher-order flow solver on a 1057 by 193 structured grid to provide a benchmark for assessing accuracy. As demonstrated in Refs. 26 and 27, the numerical error for these results is extremely small. The turbulence model, transition points, and distance to the outer boundary are all consistent. In addition to requiring sufficient boundary-layer resolution as in the preceding case, this case also requires satisfactory resolution of the shock wave that forms on the upper surface. A grid of approximately 8000 nodes with 128 points on the airfoil was adapted with a single pass to yield a grid of approximately 17,000 nodes. Solutions were also computed using unadapted grids of 17,000 and 52,000 nodes, the latter showing fair agreement with the benchmark data. The results shown in Fig. 12 show that the adapted 17,000 node grid produces a surface pressure that lies reasonably close to that obtained on the unadapted grid with 52,000 nodes. In comparison to the structured grid results, the adapted grid provides a reasonable approximation given the number of nodes used.

The final test case is the high lift airfoil case L1T2 in Ref. 24, which includes a 12.5%c leading-edge slat and a 33%c single-slotted flap, where c is the chord length of the nested configuration. The slat is located in the optimum position at an angle of 25 deg, and the flap angle is 20 deg. This geometry is typical of a takeoff configuration. Experimental surface pressures are available along the transverse profiles of total pressure at three locations. Excellent agreement with the experimental data for this geometry can be obtained using the Spalart–Allmaras turbulence model on well-refined multiblock structured grids, as shown in Ref. 28. The data computed on such well-refined structured grids are again used to provide a benchmark.

Adaptive gridding can be particularly useful in the computation of flows over high-lift, multielement airfoil configurations, due to the need to resolve merging boundary layers and wakes. Figure 13 shows the adapted grid near the trailing edge of the main airfoil with the viscous regions receiving the majority of the adaptive enhancement compared to the original unadapted grid in Fig. 14. Figure 15 compares the surface pressures obtained on the multiblock structured grid of Ref. 28 with those obtained on adapted and unadapted grids of roughly 84,000 nodes. The adapted grid produces superior agreement with the benchmark data, especially on the main airfoil. Inspection of the total pressure profiles shown in Figs. 16–18 shows that the solution obtained on the adapted grid is far more accurate than that computed on the unadapted grid. As seen in Fig. 16, the unadapted grid leads to a boundary layer on the upper surface of

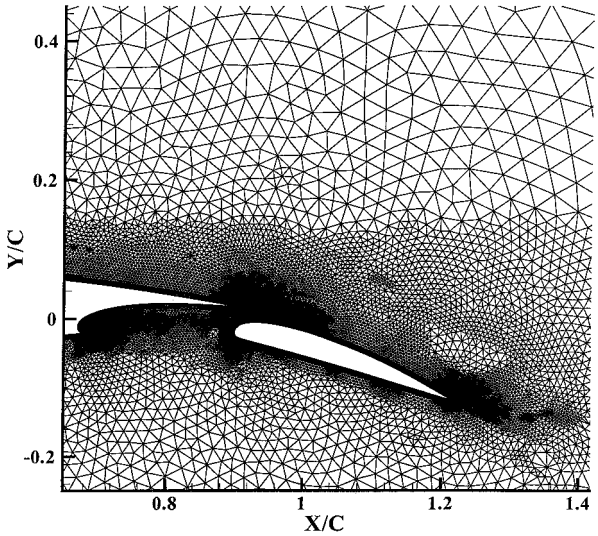

Fig. 13 Adapted grid near flap; case 4.

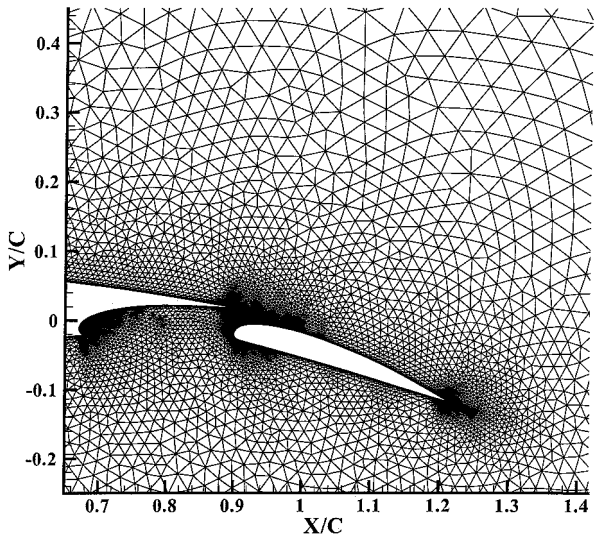

Fig. 14 Unadapted grid near flap; case 4.

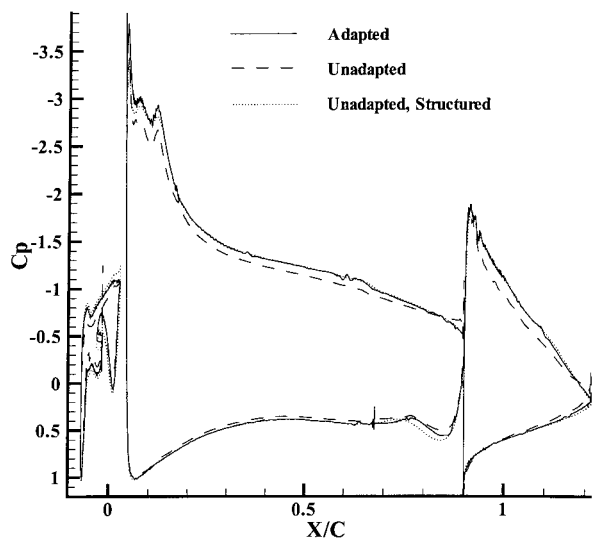

Fig. 15 Surface pressure coefficient; case 4.

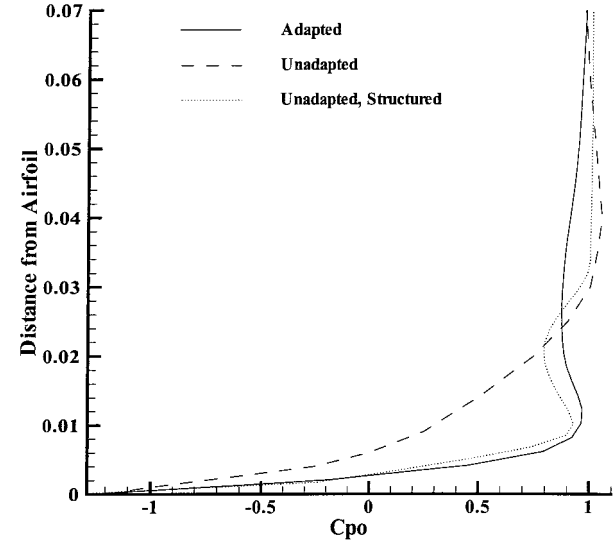

Fig. 16 Total pressure coefficient profiles at 35% chord on the mail airfoil; case 4.

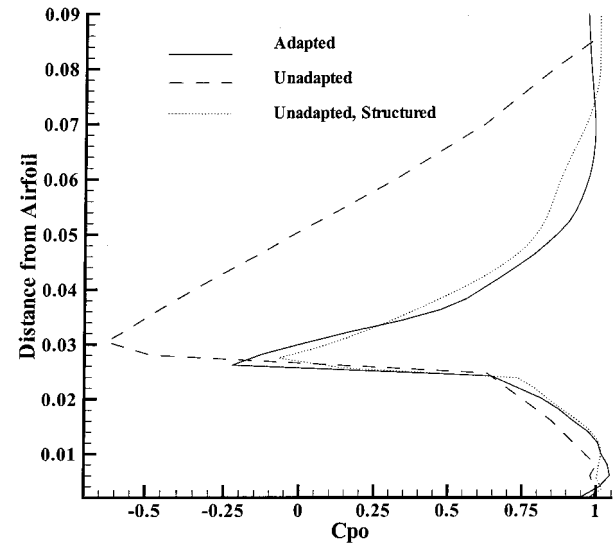

Fig. 17 Total pressure coefficient profiles at the trailing edge of the mail airfoil; case 4.

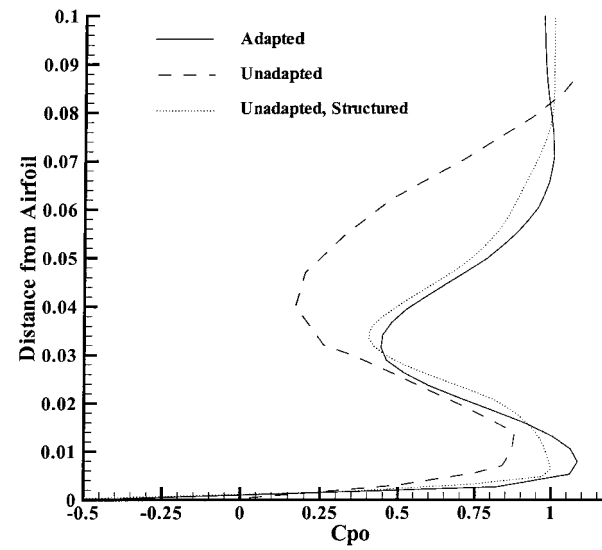

Fig. 18 Total pressure coefficient profiles at 50% chord on the flap; case 4.

the main airfoil that is much too thick, and the wake from the slat is not seen at all. The adapted grid produces reasonable agreement given the overall grid density. Figure 17 shows the same trends at the trailing edge of the main airfoil: very poor prediction of the upper surface boundary layer using the unadapted grid and excellent agreement using the adapted grid. Finally, the unadapted grid leads to a poor prediction of the wake of the main airfoil as well as the boundary layer on the upper surface of the flap, which is again too thick, as shown in Fig. 18. The adapted grid produces much better agreement in both areas. Note that these two grids have roughly the same number of nodes, and the unadapted grid is a reasonable grid generated without specific knowledge of the solution, not a globally refined grid. For this test case and case 3, the computational effort for adaptation represented approximately 3% of the total effort.

Conclusions

This paper presents three contributions toward effective solution-adaptive gridding for aerodynamic flows. They are as follows: 1) an improved artificial dissipation operator that leads to reduced error on irregular high aspect ratio triangular grids, 2) an improved retriangulation procedure applicable to highly irregular anisotropic regions of the grid, and 3) a systematic quantitative assessment of the adaptive technique for a variety of practical test cases.

The benefits of the modified Laplacian artificial dissipation operator and the solution-dependent retriangulation procedure have been demonstrated through the use of well-resolved benchmark solutions. Lift and drag comparisons with grid-independent values indicate that a substantial improvement in solution accuracy is possible for a given grid size with the adaptive algorithm outlined in this paper. The use of such a quantitative assessment of the error reduction associated with grid adaptation has been lacking in many previous studies and forms a basis on which future work can be evaluated.

References

[1]South, J. C., Jr., Thomas, J. L., and Van Rosendale, J. (eds.), "ICASE/LaRC Workshop on Adaptive Gridding Methods," NASA CP-3316, Oct. 1995.

[2]Habashi, W. G., and Fortin, M., "Anisotropic Mesh Optimization: Towards a Solver-Independent and Mesh-Independent CFD," von Kármán Inst. Lecture Series in Computational Dynamics, No. 1996-06, Concordia Univ., Montreal, PQ, Canada, Aug. 1996.

[3]Dannenhoffer, J. F., and Baron, J. R., "Grid Adaptation for the 2-D Euler Equations," AIAA Paper 85-0484, Jan. 1985.

[4]Warren, G. P., Anderson, W. K., Thomas, J. L., and Krist, S. K., "Grid Convergence for Adaptive Methods," Inst. for Computational Fluid Dynamics Conf. on Numerical Methods for Fluid Dynamics, Univ. of Reading, Reading, England, U.K., April 1992.

[5]Mavriplis, D. J., "Accurate Multigrid Solution of the Euler Equations on Unstructured and Adaptive Meshes," *AIAA Journal*, Vol. 28, No. 2, 1990, pp. 213–221.

[6]Mavriplis, D. J., "Turbulent Flow Calculations Using Unstructured and Adaptive Meshes," Inst. for Computer Applications in Science and Engineering, ICASE Rept. 90-61, Sept. 1990.

[7]Baker, T. J., "Mesh Adaptation Strategies for Problems in Fluid Dynamics," *Finite Elements in Analysis and Design*, Vol. 25, No. 3–4, 1997, pp. 243–473.

[8]Biswas, R., and Strawn, R. C., "Mesh Quality Control for Multiply-Refined Tetrahedral Grids," *Applied Numerical Mathematics*, Vol. 20, No. 4, 1996, pp. 337–348.

[9]Kallinderis, Y., "A 3-D Finite-Volume Method for the Navier–Stokes Equations with Adaptive Hybrid Grids," *Applied Numerical Mathematics*, Vol. 20, No. 4, 1996, pp. 387–406.

[10]Hall, D. J., and Zingg, D. W., "Viscous Airfoil Computations Using Adaptive Grid Redistribution," *AIAA Journal*, Vol. 33, No. 7, 1995, pp. 1205–1210.

[11]Jameson, A., Schmidt, D., and Turkel, E., "Numerical Solution of the Euler Equations by Finite Volume Methods Using Runge-Kutta Time-Stepping Schemes," AIAA Paper 81-1259, June 1981.

[12]Spalart, P. R., and Allmaras, S. R., "A One-Equation Turbulence Model for Aerodynamic Flows," AIAA Paper 92-0439, Jan. 1992.

[13]Mavriplis, D. J., and Jameson, A., "Multigrid Solution of the Navier–Stokes Equations on Triangular Meshes," *AIAA Journal*, Vol. 28, No. 8, 1990, pp. 1415–1425.

[14]Lindquist, D. R., "A Comparison of Numerical Schemes on Triangular and Quadrilateral Meshes," Computational Fluid Dynamics Lab., CFDL-TR-88-6, Massachusetts Inst. of Technology, Cambridge, MA, May 1988.

[15]Walsh, P., and Zingg, D. W., "A Solution-Adaptive Solver for Aerodynamic Applications Using Unstructured Grids," *Proceedings of the Fourth Annual Conference of the CFD Society of Canada*, Computational Fluid Dynamics Society of Canada, Ottawa, ON, Canada, 1996, pp. 161–168.

[16]Walsh, P., and Zingg, D. W., "On the Accuracy of Viscous Airfoil Computations Using Solution-Adaptive Unstructured Grids," AIAA Paper 97-0329, Jan. 1997.

[17]Walsh, P., "Adaptive Solution of Viscous Aerodynamic Flows Using Unstructured Grids," Ph.D. Dissertation, Inst. for Aerospace Studies, Univ. of Toronto, Downsview, ON, Canada, Dec. 1997.

[18]Parthasarathy, V., and Kallinderis, Y., "New Multigrid Approach for Three-Dimensional Unstructured, Adaptive Grids," *AIAA Journal*, Vol. 32, No. 5, 1994, pp. 956–963.

[19]Parthasarathy, V., and Kallinderis, Y., "Adaptive Prismatic-Tetrahedral Grid Refinement and Redistribution for Viscous Flows," *AIAA Journal*, Vol. 34, No. 4, 1996, pp. 707–716.

[20]Mavriplis, D., "Unstructured and Adaptive Mesh Generation for High Reynolds Number Viscous Flows," NASA, Inst. for Computer Applications in Science and Engineering, ICASE, Rept. 187534, Feb. 1991.

[21]Barth, T. J., "Aspects of Unstructured Grids and Finite Volume Solvers for the Euler and Navier–Stokes Equations," *Computational Fluid Dynamics*, von Kármán Inst. Lecture Series, No. 1994-05, Vol. 1, 1994.

[22]Bristeau, M. O., Glowiniski, R., Periaux, J., and Viviand, H., *Numerical Simulation of Compressible Navier–Stokes Flows: A GAMM Workshop*, Friedr. Vieweg and Son, Braunschweig, Germany, 1985, pp. 3–23.

[23]Cook, P. H., McDonald, M. A., and Firmin, M. C. P., "Test Cases for Inviscid Flow Field Methods," AGARD Advisory Rept. 138, May, 1985, pp. A6-1–A6-77.

[24]Burt, M., "A Selection of Experimental Test Cases for the Validation of CFD Codes," AGARD Advisory Rept. 303, Vol. 1, 2, Aug. 1994, pp. 58, 59.

[25]Fejtek, I. G., "Summary of Code Validation Results for a Multiple Element Airfoil Test Case," AIAA Paper 97-1932, June–July 1997.

[26]De Rango, S., and Zingg, D. W., "Aerodynamic Computations Using a Higher-Order Algorithm," AIAA Paper 99-0167, Jan. 1999.

[27]Zingg, D. W., De Rango, S., Nemec, M., and Pulliam, T. H., "Comparison of Several Spatial Discretizations for the Navier–Stokes Equations," AIAA Paper 99-3260, June–July 1999.

[28]Nelson, T. E., Godin, P., De Rango, S., and Zingg, D. W., "Flow Computations for a Three-Element Airfoil System," *Canadian Aeronautics and Space Institute Journal*, Vol. 45, No. 2, 1999, pp. 132–139.

J. Kallinderis
Associate Editor